Engineering Structures 39 (2012) 162–175

Contents lists available at SciVerse ScienceDirect

Engineering Structures

journal homepage: www.elsevier.com/locate/engstruct

Behaviour of steel-fibre-reinforced normal-strength concrete slender columns under cyclic loading

K.E. Caballero-Morrison, J.L. Bonet *, Juan Navarro-Gregori, J.R. Martí-Vargas

Instituto de Ciencia y Tecnología del Hormigón, Universitat Politècnica de València, Camino de Vera s/n, 46022 Valencia, Spain

ARTICLE INFO

Article history:
Received 25 June 2011
Revised 15 December 2011
Accepted 5 February 2012
Available online 28 March 2012

Keywords:
Slender column
Confined concrete
Reinforced concrete
Steel fibre
Ductility
Energy dissipation
Strength
Axial load
Cyclic load

ABSTRACT

The inclusion of ductility requirements is necessary to guarantee the safety design of any concrete structure subjected to unexpected and/or reversal loads. It is important to outline that plastic hinges may be developed in columns of reinforced concrete buildings, especially in column-foundation joints. The deformation capacity of the column depends on its slenderness. However, few experimental tests of normal and fibre-reinforced concrete columns in the range of medium slenderness (between 5 and 10) have been performed for the case of cyclic loading. This paper presents an experimental research study on the behaviour of slender columns subjected to combinations of constant axial and lateral cyclic loads. In order to study the behaviour of this type of element fourteen experimental tests were performed. The experimental results make it possible to calibrate numerical models, and to validate simplified methods. The following variables are studied: slenderness, axial load level, transverse reinforcement ratio, and volumetric steel-fibre ratio. The maximum load and deformation capacity of the columns are analyzed. It is interesting to note that the deformation capacity depends on the four test variables analyzed. Moreover, the inclusion of steel fibres into the concrete mixture increases the deformation capacity. The inclusion of a minimum transverse reinforcement is required in order to improve the effectiveness of the steel fibres. Thus, the column behaviour suffers moderate strength losses due to cyclic loads. Finally, slenderness influences the deformation capacity if second-order effects are important, the cross-section displays ductile behaviour, and the capacity of the materials is reached.

1. Introduction

Structures with ductile behaviour have the capacity to absorb and dissipate energy under accidental loads, without a significant loss of strength. This inelastic behaviour is due to the development of plastic hinges. The capacity of ductile structures to dissipate energy is taken into account in the seismic design of concrete structures. Nowadays, the criterion of capacity-based design (EC-8 [14], FEMA P-750 [17]) is used in the seismic design of structures. This criterion is based on the protection of the fragile elements and regions of the structure, which are strengthened in comparison to the ductile ones. As a result, ductile failure mechanisms can be reached more easily. For this reason, it is necessary to guarantee that plastic hinges are developed earlier in the beams than in the columns ('strong column – weak beam'). However, according to ACI 441R-97 [3], it has been stated that hinges should appear at the ends of the columns after an earthquake [20]. Consequently, reinforced concrete columns have to provide an important inelastic response without a significant decrease of strength capacity, particularly in bridge columns or in column-foundation joints.

In order to guarantee the ductile behaviour of the columns, EC-8 [14], and ACI-318(08) [1] codes specify the transverse reinforcement ratio to be included in critical zones where a plastic hinge could be developed. For high levels of axial force it is necessary to include a significant amount of transverse reinforcement. This may cause difficulties while concrete is being cast. A possible solution to this problem [29] is adding steel fibres to the concrete mixture. The combined use of steel fibres and transverse reinforcement can reduce the transverse reinforcement ratios required by design codes, particularly in the case of seismic design. However, the expressions proposed in the codes disregard the favourable effect of steel fibres (EC-8 [14], ACI-318(08) [1]).

Several authors have studied the behaviour of fibre-reinforced normal-strength concrete (e.g. [16,15,25]). These studies show the typical stress-strain constitutive equations of the concrete in compression, in which the inclusion of steel fibres represents a minor increase in peak stress, a significant increase in the strain corresponding to peak stress, and a substantial toughness increase. This is reflected in an increase of the total energy the material absorbs prior to failure. Recent research (e.g. [18,4,9,28]) has shown that the presence of steel fibres delays concrete spalling, and increases the deformation capacity of concrete columns subjected to compressive axial load, or combinations of axial load and

* Corresponding author. Tel.: +34 96 387 7007x75615; fax: +34 96 387 7569.
E-mail address: jlbonet@cst.upv.es (J.L. Bonet).

0141-0296/$ - see front matter © 2012 Elsevier Ltd. All rights reserved.
doi:10.1016/j.engstruct.2012.02.003

constant eccentricity. Lately, several design codes (NZS 3101: Part: 2006 [31], CNR-DT 204/2006 [12], ACI-318(08) [1], EHE-08 [11], ACI 544.4R-88 (Reapproved 2009) [2], MC-2010 [21] among others) have included prescriptions concerning the use of fibre-reinforced concrete such as description of materials properties, design procedures or detailing provisions.

There are numerous publications concerning the study of the strength and deformation capacity of columns under cyclic loading [8,10]. Experimental tests available are focused on reinforced concrete columns (without fibres) with shear slenderness (λ_V) below 6.5 [27]. Laboratory tests of steel-fibre concrete columns subjected to combination of axial and lateral loads have not been reported so far.

Second-order effects (P–Δ effects) have an influence on the deformation capacity of slender columns [5], and there is also a lack of experimental work on columns with slenderness over 6.5. As a result, it is necessary to study the load and deformation capacities of reinforced concrete slender columns subjected to constant axial load combined with monotonic or cyclic lateral loads.

In this research work an experimental program is presented to fill the gap existing in the literature on slender normal-strength concrete column tests, including or excluding steel fibres, under constant axial and cyclic loads.

In order to analyze the effect of confinement and the inclusion of steel fibres, the variables considered in the test program are the axial load level and the slenderness of the column. The experimental tests provide results on the general behaviour, deformation, energy dissipation, and strength capacity of the column. In addition, the results make it possible to calibrate numerical models, and to validate simplified methods proposed in the codes.

2. Test program

Test specimens were designed to represent two semi-columns of two adjacent storeys connected by a central element (stub). This can simulate the stiffening effect of an intermediate slab, or a column-foundation joint represented by the central element of the specimen. Fig. 1 shows the geometric details of the specimens. The length of each semi-column (L_s) is greater than the potential length of a plastic hinge (ACI-318(08) [1], EC-8 [14]). Fig. 2 shows cross-section details of the semi-columns. This type of specimen has already been employed by Yamashiro and Sies [37], Priestley and Park [30] and Barrera et al. [7] among others.

The distribution of the longitudinal reinforcement remains constant along the specimen. The ratio between the mechanical concrete cover (distance from the centroid of the tensile bar to the outer surface of the concrete) and the total depth of the section is 0.15. All the stirrups were anchored with 135° bends extending 50 mm ($6.25\phi_t$, where ϕ_t is the nominal diameter of the stirrup) into the concrete core. This length satisfies the requirements of EC-2 [13] ($5\phi_t > 50$ mm) and ACI-318(08) [1] ($6\phi_t$), even though it is less than the minimum length reported in ACI-318(08) [1] for the case of seismic actions (76 mm). Spanish code EHE-08 [11] does not take this design detail into account.

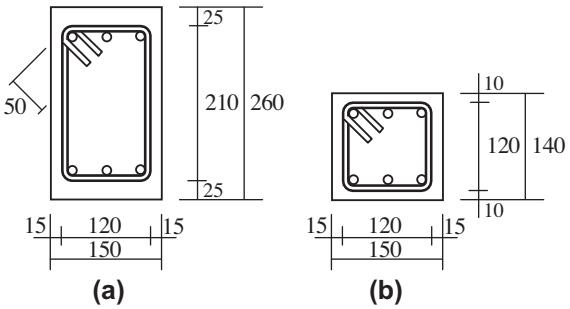

Fig. 2. Cross-section details (unit: mm).

The parameters analyzed are: (a) shear slenderness ($\lambda_V = L_s/h = M/(V \cdot h)$, where h is the total depth of the cross-section, M and V are the bending moment, and the shear load applied); (b) the relative normal force ($\nu = N/[b \cdot h \cdot f_c]$, where N is the axial load applied, b is the width of the cross-section, and f_c is the concrete compressive strength); (c) the confinement effectiveness of the transverse reinforcement ($\alpha \cdot \omega_\omega$, where α is the confinement effectiveness factor, this factor takes into account the spacing and the arrangement of the stirrups in the section, and ω_ω is the volumetric transverse reinforcement ratio (EC-8 [14] Section 5.4.3.2.2)); and (d) the steel-fibre content.

In the experimental program each parameter studied ranges as follows:

- Concrete strength (f_c). A nominal strength of 30 MPa has been chosen.
- Shear slenderness ratio (λ_V). Values of 5.77 and 10.71 have been taken into account. Second-order effects cannot be neglected in either case, and the values chosen are greater than those reported in the literature. EC-8 [14] code can be applied to columns with shear slenderness below 10. Columns with slightly higher ratios than those reported in this code are analyzed.
- Relative normal force (ν). The following three levels have been considered: 0.10, 0.35 and 0.55. The minimum and maximum values correspond to the limits in accordance with EHE-08 [11], EC-8 [14], and ACI-318 (08) [1]. In EC-8 [14] code it is stated that the relative normal force cannot exceed 0.65 when designing columns with medium-ductility (DCM), and 0.55 for the case of high-ductility (DCH). Moreover, according to EHE-08 (Annex 10) [11], and ACI-318(08) (21.6.1) [1], the minimum relative normal force to be considered in columns under seismic actions is 0.10.
- Longitudinal reinforcement ratio (ρ_l). Two similar values have been considered: 1.44% if $\lambda_V = 10.71$ and 1.74% if $\lambda_V = 5.77$. The objective is to compare the deformation capacity in all tests while the other parameters remain constant.

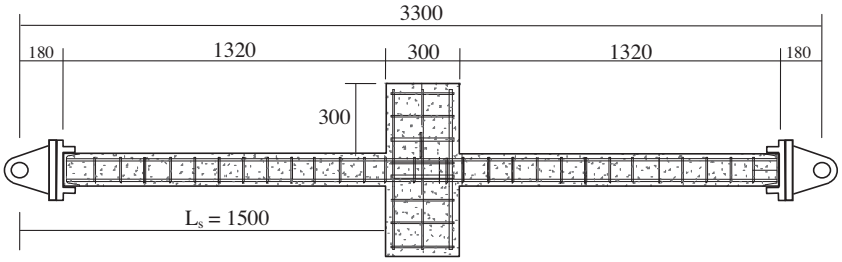

Fig. 1. Dimensions of test specimens (unit: mm).

Table 1
Details of test specimens.

Id	Specimen	h (m)	b (m)	λ_V	f_c (MPa)	N (kN)	$\frac{N}{b \cdot h \cdot f_c}$	Reinforcement				
								Longitudinal		Transverse (ϕ_t = 8 mm)		
								$\phi_{l\ (mm)}$	ρ_l (%)	s_t (mm)	ρ_S (%)	$\alpha \cdot \omega_\omega$
N1	NF00L05V2S100	0.26	0.15	5.77	33.57	491.7	0.38	6ϕ12	1.74	100	1.40	0.04
N2	NF00L05V2S50	0.26	0.15	5.77	29.68	413.9	0.36	6ϕ12	1.74	50	2.79	0.13
N3	NF00L05V1S50	0.26	0.15	5.77	29.18	138.2	0.12	6ϕ12	1.74	50	2.79	0.14
N4	NF00L10V2S70	0.14	0.15	10.71	30.63	211.2	0.33	6ϕ8	1.44	70	2.56	0.11
N5	NF00L05V3S50	0.26	0.15	5.77	30.40	637.9	0.54	6ϕ12	1.74	50	2.79	0.13
N6	NF00L10V3S70	0.14	0.15	10.71	32.68	347.0	0.51	6ϕ8	1.44	70	2.56	0.10
N7	NF30L05V2S100	0.26	0.15	5.77	33.37	473.8	0.36	6ϕ12	1.74	100	1.40	0.04
N8	NF30L05V2S50	0.26	0.15	5.77	38.00	523.3	0.35	6ϕ12	1.74	50	2.79	0.10
N9	NF60L05V2S100	0.26	0.15	5.77	33.65	412.7	0.31	6ϕ12	1.74	100	1.40	0.04
N10	NF60L05V2S50	0.26	0.15	5.77	29.52	448.6	0.39	6ϕ12	1.74	50	2.79	0.13
N11	NF60L05V2S600	0.26	0.15	5.77	32.12	420.6	0.34	6ϕ12	1.74	600	0.23	0.01
N12	NF60L10V2S70	0.14	0.15	10.71	30.35	241.4	0.38	6ϕ8	1.44	70	2.56	0.11
N13	NF60L10V1S70	0.14	0.15	10.71	30.78	107.9	0.17	6ϕ8	1.44	70	2.56	0.11
N14	NF60L05V1S50	0.26	0.15	5.77	32.43	153.4	0.12	6ϕ12	1.74	50	2.79	0.12

- Effective volumetric mechanical ratio of confinement ($\alpha \cdot \omega_\omega$). Three levels are taken into account: high (0.12), medium (0.04) and low (0.01). Given a transverse reinforcement diameter ϕ_t = 8 mm: (a) $\alpha \cdot \omega_\omega$ = 0.12 is obtained assuming a transverse reinforcement spacing (s_t) of 50 mm if λ_V = 5.77, and s_t = 70 mm if λ_V = 10.71; (b) $\alpha \cdot \omega_\omega$ = 0.04 is obtained with s_t = 100 mm if λ_V = 5.77, and s_t = 70 mm if λ_V = 10.71; and (c) $\alpha \cdot \omega_\omega$ = 0.01 taking s_t = 600 mm if λ_V = 5.77. The latter level is considered for analysis if it is possible to replace the transverse reinforcement with steel fibres, for cases with a larger volume of steel fibres.
- Steel-fibre content: 30 and 60 kg/m^3, corresponding to volumetric steel-fibre ratios of 0.38% and 0.76% respectively.

Table 1 shows the details of the 14 specimens included in the experimental program. Designation of the specimens is carried out using *NFxLyVzSk*, where '*x*' denotes the fibre content (00, 30 or 60 kg/m^3), '*y*' is the shear slenderness (L05 for λ_V = 5.77 and L10 for λ_V = 10.71), '*z*' is the relative normal force (V1 for v = 0.10, V2 for v = 0.35 and V3 for v = 0.55), and '*k*' is the transverse reinforcement spacing (s_t) in mm.

Specimens were cast horizontally in externally-vibrated forms, and stripped after 24 h. Furthermore, they were kept horizontal in a humid environment to minimize the effects of shrinkage, and were all tested at 28 days. To determine the average concrete compressive strength (f_c) three cylinders (150 × 300 mm) (UNE-EN 12390-3 [33]) were tested for each specimen.

2.1. Material properties

Concrete: Portland type CEM I 52,5R Cement (UNE-EN 197-1:2000 [35]) was used, and additives were included for fibre-reinforced concrete. Aggregates used were crushed limestone gravel with sizes ranging from 4 to 7 mm, and the water-cement ratio considered was 0.63. Table 2 lists the dosages taken into account.

Steel: Type B 500 SD (EHE-08 [11]) and C class (EC-2 [13]) were used. Fig. 3 shows the results of the characterization tests (UNE EN-10002-1 [32]). To determine the average values of the steel mechanical properties two pieces of reinforcing steel were tested for each nominal diameter.

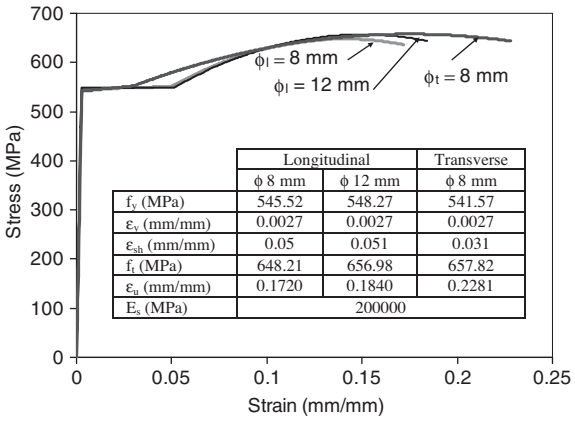

	Longitudinal		Transverse
	ϕ 8 mm	ϕ 12 mm	ϕ 8 mm
f_y (MPa)	545.52	548.27	541.57
ε_y (mm/mm)	0.0027	0.0027	0.0027
ε_{sh} (mm/mm)	0.05	0.051	0.031
f_t (MPa)	648.21	656.98	657.82
ε_u (mm/mm)	0.1720	0.1840	0.2281
E_s (MPa)	200000		

Fig. 3. Stress–strain behaviour of steel.

Steel fibres: Type: DRAMIX RC-65/35-BN steel fibres, with aspect ratio l/d = 35/0.55 = 63.63, and 1100 MPa tensile strength were used. A 550 × 150 × 150 mm^3 prismatic specimen was made for each mixture, and a 3-point bending test was performed according to UNE-EN 14651:2007 [34] in order to determine the corresponding limit of proportionality (f_L), and the residual flexural tensile strength (f_{Rj}) (see Table 3).

2.2. Test setup

A steel-loading frame was designed to perform the tests, as shown in Fig. 4a. The horizontal loading system comprises a 2500 kN hydraulic actuator (Fig. 4b), which is part of a frame composed of four longitudinal bars anchored to plates at the ends. The hydraulic jack is positioned in series with the test specimen, and reacts on one of the plates. The load is transmitted to the frame plate located at the opposite end of the specimen by the longitudinal bars.

Table 2
Concrete dosages considered (kg/m^3).

Concrete type	Cement	Water	Sand	Crushed limestone	Steel fibres	Plasticizer 651N (%)	Superplasticizer glenium AC31 (%)
1	348	220	1065	666	–	–	–
2					30	1.22	2.44
3					60	1.57	3.13

Table 3
Results of bending tests.

Id	Specimen	f_L (MPa)	f_{R1} (MPa)	f_{R2} (MPa)	f_{R3} (MPa)	f_{R4} (MPa)
N7	NF30L05V2S100	2.89	2.89	2.90	2.91	2.91
N8	NF30L05V2S50	3.03	2.88	3.39	3.48	3.06
N9	NF60L05V2S100	4.41	6.51	7.24	7.18	6.37
N10	NF60L05V2S50	4.96	6.27	7.02	6.77	6.19
N11	NF60L05V2S600	4.35	6.59	7.80	7.46	6.58
N12	NF60L10V2S70	4.45	6.74	8.10	7.52	6.69
N13	NF60L10V1S70	5.00	7.79	8.78	7.97	7.02
N14	NF60L05V1S50	4.39	7.30	8.83	8.15	6.97

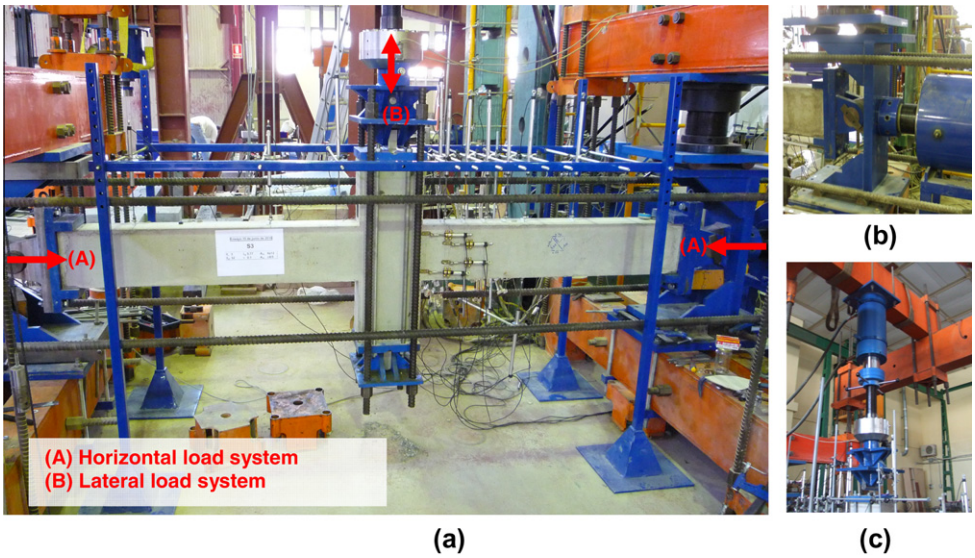

Fig. 4. Experimental setup and testing frame.

A sliding support allows horizontal movement in the hydraulic actuator.

Steel joints have been positioned at the ends of the specimen to allow the condition of pin end, and to ensure that the horizontal load is always applied on the central axis of the element. These joints are supported on a plate with a roller that allows the horizontal displacement of the specimen (Fig. 4b). The longitudinal reinforcement of the column has been welded at each end to a UPN steel profile, which is fixed to the support system with four embedded screws.

The lateral loading system is fixed to an auxiliary frame that transmits lateral loads to the test slab (Fig. 4c). The lateral load is applied to the specimen by a 500 kN double effect hydraulic jack.

The forces applied by the hydraulic actuators are controlled by two load cells: a 2000 kN cell, attached to a plate in the horizontal loading system frame, and a 500 kN cell, between the specimen and the hydraulic actuator of the lateral load system.

2.3. Instrumentation

Strain gauges were placed in eight sections at only one side of the specimen. To ensure that the instrumented side was the first to reach failure, an additional longitudinal bar was positioned at both borders of a section at a distance greater than the potential length of the plastic hinge. These strain gauges are glued to the central bar, both in the compressed and the tensile reinforcement (Fig. 5).

In addition, 15 linear variable displacement transformers (LVDTs) were used to measure displacements. Devices 1–10 are designed to record the lateral displacement of the specimen (Fig. 6). The rotation of the central element is obtained from the records of devices number 7 and 8. LVDT number 11 records the possible transverse displacement of the specimen due to possible geometrical imperfections or lateral instability (Fig. 6). During the tests, this effect was observed as negligible even when the damage level was very high. LVDTs 12–15 (Fig. 7), are designed to indirectly record the average bending curvature at 70 mm and at 170 mm from the column-stub interface. The average curvature at section i (φ_i) is measured as:

$$\varphi_i = \frac{\delta_{ij}/100 - \delta_{ik}/100}{z_i} \quad (1)$$

where δ_{ij} is the measured displacement of LVDT–no. j at the top side (LVDT number 14 or number 16); δ_{ik} is the measured displacement of LVDT–no. k at the bottom side (LVDT number 13 or number 15), and z_i is the distance between the top and the bottom LVDT locations (all displacements are in mm).

2.4. Test procedure

First, a horizontal load corresponding to the relative normal force is applied, and kept constant throughout the test. The lateral load is then applied.

The first load cycle is done with load-control capabilities until the total bending moment (M_{cs}) is 75% of the ultimate bending moment (M_u) at the critical section (70 mm from the column-stub interface, see Fig. 8) in each direction of the tip displacement (Δ^{+1} and Δ^{-1}). The ultimate bending moment is calculated

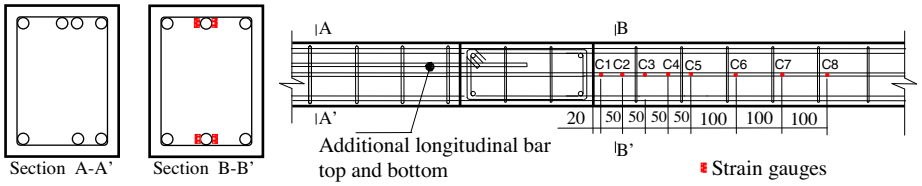

Fig. 5. Top view of the strain gauges disposal (unit: mm).

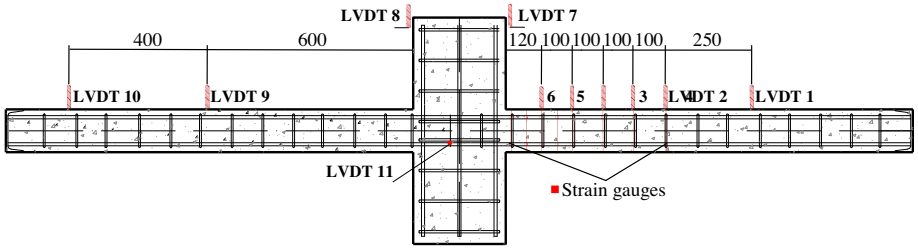

Fig. 6. Lateral displacement measurements (unit: mm).

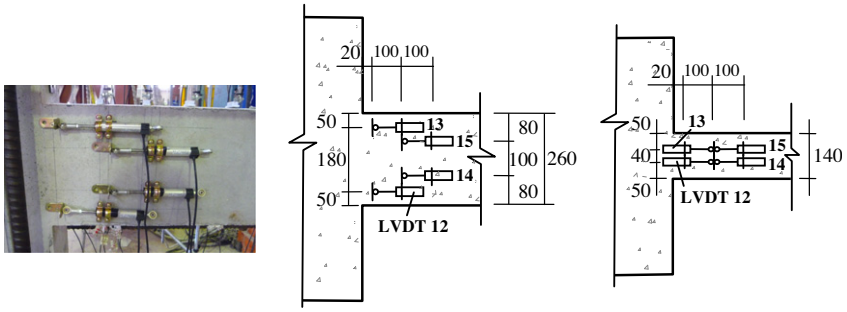

Fig. 7. Horizontal displacement measurements (unit: mm).

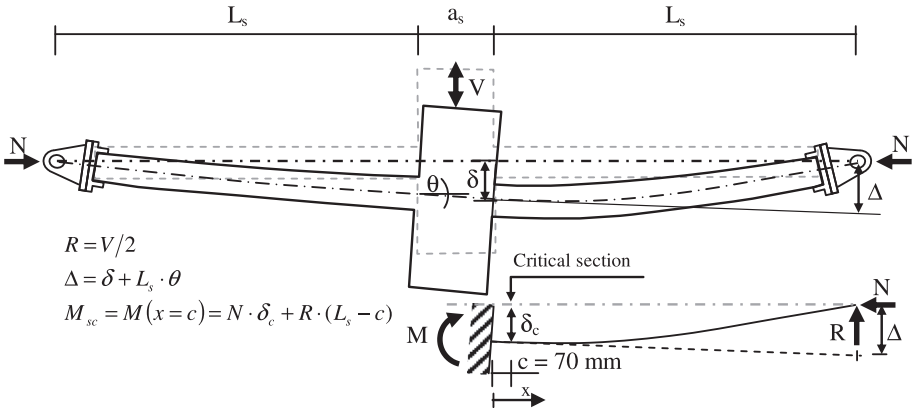

Fig. 8. Specimen idealization.

according to EC-2 [10]. This takes into account the properties of the materials and the axial force pre-applied. The effect of confinement of concrete and steel fibres is neglected, and safety factors are taken to equal one. During the first cycle, the maximum and minimum displacements at the ends of the column can be obtained (Δ^{+1} and Δ^{-1}, at $0.75 \cdot M_u$ and $-0.75 \cdot M_u$, respectively, Fig. 9). The nominal elastic displacement Δ_y is calculated on the basis of the following expression [19]:

$$\Delta_y = \frac{4}{3} \cdot \frac{\Delta_1^+ + |\Delta_1^-|}{2} \tag{2}$$

The following cycles are performed with load-displacement control. The displacement imposed is obtained as $\Delta = \mu \Delta_y$, where μ is the nominal displacement ductility factor. Thus, at the beginning of the second cycle $\mu = 1$, and then Δ increases Δ_y every two cycles [19] (Fig. 9). Fig. 8 shows how to calculate Δ displacement at the end of the column and the total bending moment (M_{cs}) at the critical section.

A conventional failure criterion has been fixed, assuming a 20% loss of strength capacity in terms of lateral load or bending moment [19,29]. This has been applied to all the tests performed.

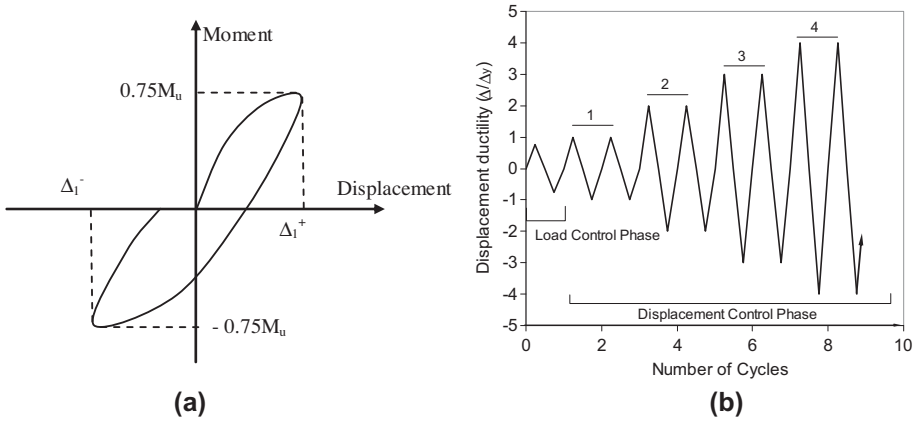

Fig. 9. Test procedure. (a) Determination of Δ_l^+ and Δ_l^- from the first elastic cycle under load control. (b) Loading history.

3. Test results and observations

Figs. 10 and 11 show the load–displacement diagrams recorded, and Table 4 shows a summary of the main test results.

3.1. General behaviour

The following general observations have been made:

1. Concrete cover spalled in all specimens (Figs. 10 and 11). This was more visible in the specimens without fibres. In addition, fibre-reinforced concrete specimens achieved μ values higher than those without fibres, except for NF60L05V2S600 (Fig. 10g).
2. Longitudinal reinforcement yielded in all specimens (Figs. 10 and 11). In addition, the absolute value of the strain in the tensile steel bars is higher than in compression, except for specimens NF00L10V3S70 and NF00L05V3S50, with $v = 0.55$.
3. The critical region length of each column specimen was evaluated by the physical observation method proposed by Pam and Ho [26]. According to these authors "*the critical region length is considered to have occurred within an extent of region that suffers the following damage: (1) spalling of concrete cover (2) penetration of spalling into concrete core region (3) local buckling of longitudinal steel (4) inelastic deformation of transverse steel; and (5) yielding of longitudinal steel (if visible)*". The l_{cr}/h ratio (critical region length (l_{cr}) and total depth of the section (h)) increases with slenderness, axial force applied, and transverse reinforcement spacing (Table 4). This length (l_{cr}) ranges between $0.62{\cdot}h$ (for $\lambda_V = 5.77$ and $v = 0.10$) and $1.71{\cdot}h$ (for $\lambda_V = 10.71$ and $v = 0.55$).
4. Nonfibrous specimens suffered major damages (Fig. 12a), and crack orientation is vertical in most cases. In fibrous specimens the crack distribution is more smeared (Fig. 12b), with the exception of NF60L05V2S600. In this specimen a typical shear failure occurred after stirrup yielding, spalling of concrete cover, and buckling of the longitudinal bars (Fig. 12c).
5. The section that connects the stub and the semi-columns was not damaged in most specimens (stub effect), despite being subjected to the maximum bending moment (Fig. 12). According to other authors like [29,22] this fact is explained by the confinement effect caused by the central element in the nearby sections, resulting in an increase of their ultimate bending moment. For this reason, the critical section is positioned 70 mm away from the central element within the critical region zone (Fig. 8). Therefore, the moment – curvature diagram is calculated at 70 mm from the column-stub interface.
6. Failure was generally reached in most tests for a lateral load producing a 20% loss of strength capacity. After conventional failure was reached, the failure of the longitudinal reinforcement occurred for $\mu = 8$ (Fig. 11c) only for specimen NF00L10V2S70.
7. The anchorage of the transverse reinforcement has been effective in all specimens, that is, stirrup hooks have not opened. Thus, the confinement produced and the deformation capacity of the specimen did not decrease.
8. It was found that buckling of the longitudinal reinforcement has an important influence on the deformation capacity of the column. This occurred when the reinforcement yielded (since this significantly decreased the stiffness of the reinforcement), and the concrete cover spalled. Rebar buckling was observed in the following cases: all columns with $s_t = 100$ mm and $s_t = 70$ mm (except for NF60L10V1S70) if $\mu > 5$, and columns with $s_t = 50$ mm if $\mu > 3$ (nonfibrous specimens) or $\mu > 5$ (fibrous specimens). The delay in this behaviour is due to the fact that buckling occurs when there is greater nominal ductility in fibrous specimens.

Therefore, the buckling of the reinforcement in compression depends on the nominal displacement ductility factor, the type of concrete (with or without fibres), the longitudinal reinforcement diameter, and the stirrup spacing. EC-8 [14] points out several stirrup spacings on the basis of the ductility required in order to prevent reinforcement buckling after concrete cover spalling ($8\phi_l$ for DCM and $6\phi_l$ for DCH, where ϕ_l is the minimum diameter of the reinforcement in compression). EHE-08 [9] code keeps the same limitations included in EC-8 [11]. However, ACI-318 (08) [1] proposes a single maximum spacing, equal to $6\phi_l$, which is not dependent on ductility. It can be seen that codes are on the unsafe side (Table 4) for the most restrictive limitation ($6\phi_l$), when $\phi_l = 12$ mm and $s_t = 50$ mm ($<6\phi_l = 72$ mm). Moreover, none of them considers a separation distance depending on the steel-fibre content. As a result, it will be necessary to carry out future experimental tests.

3.2. Ductility and energy dissipation

The ductility parameters were obtained from the idealization of the real envelope diagram [29,19]. Both the load–isplacement (V–Δ) and the bending moment–curvature (M–φ) curves are idealized in a bilinear diagram, consisting of an elastic branch and an inelastic descending branch (Fig. 13). The elastic branch starts at the origin, intersects with the real envelope curve (V–Δ or M–φ) up to 75% of V_{max} or M_{max}, and ends in V_{max} or M_{max}. Thus, the

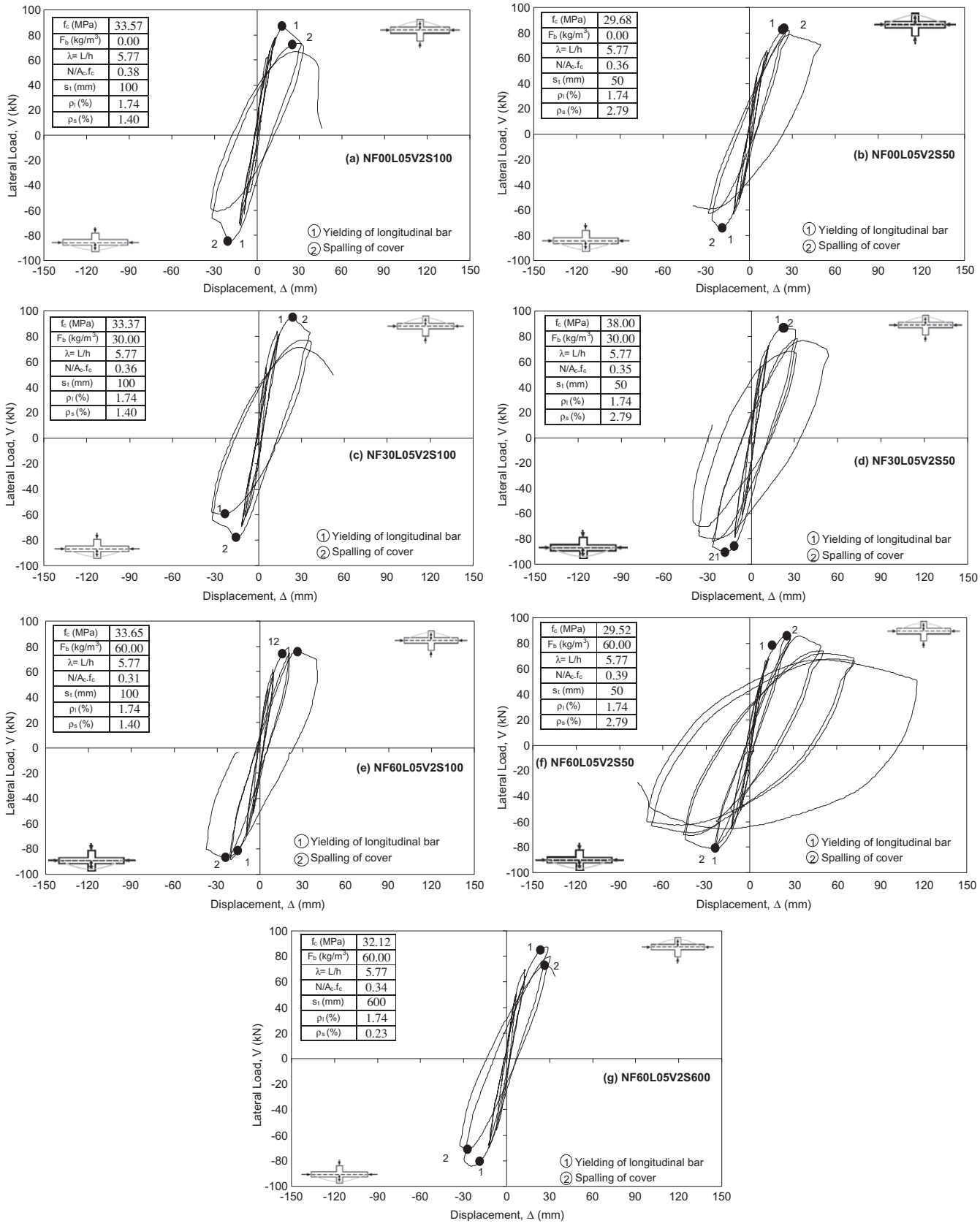

Fig. 10. Lateral load versus tip displacement. Effect of transverse reinforcement and steel fibres.

abscissa corresponding to the ideal displacement (Δ_{yI}) or the ideal elastic curvature (φ_{yI}) can be determined. The ultimate displacement (Δ_u) or the ultimate curvature (φ_u) in the real envelope curve correspond to the situation of conventional failure (20% loss of

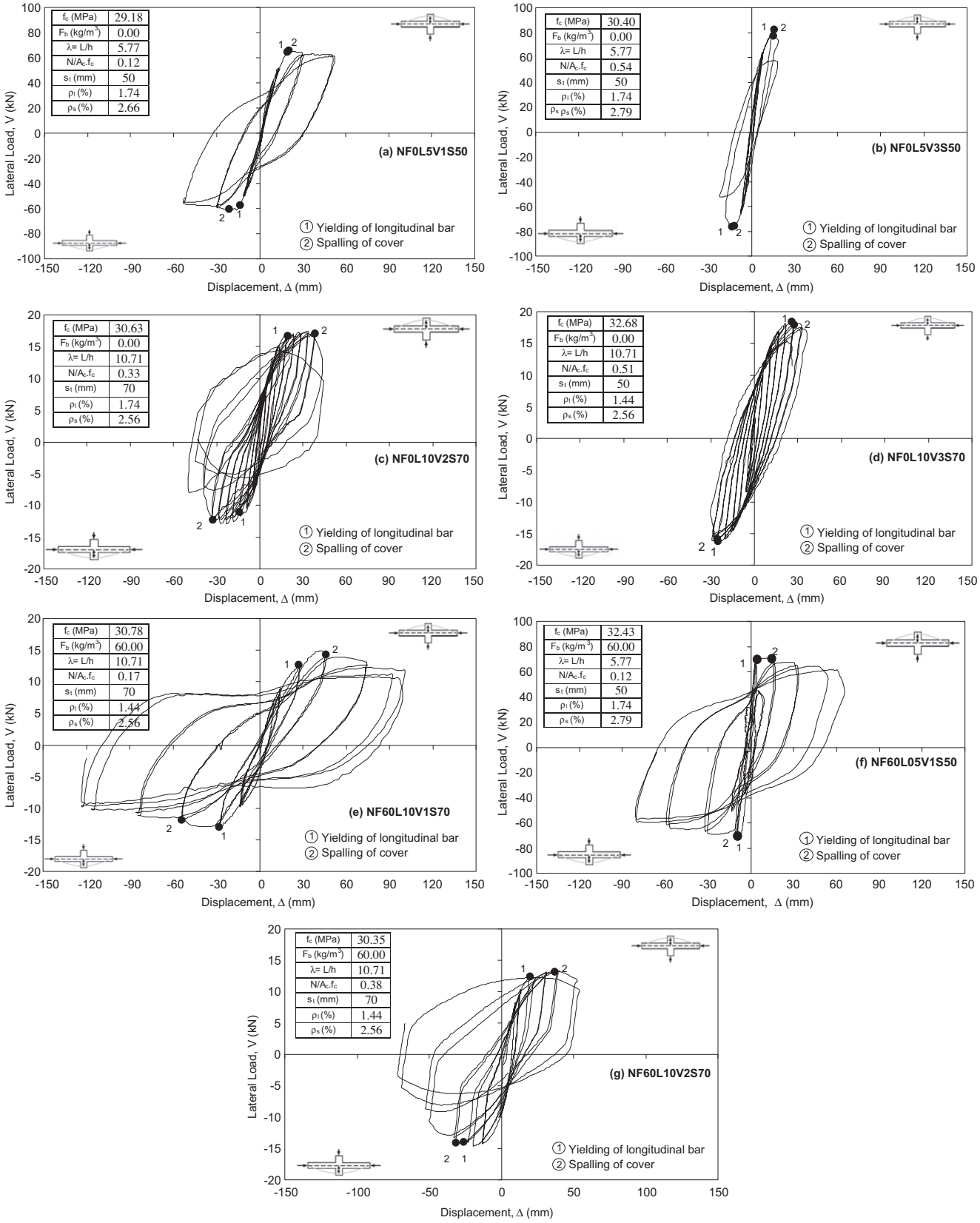

Fig. 11. Lateral load versus tip displacement. Effect of slenderness, axial load level, and steel fibres .

capacity), or maximum displacement or curvature recorded if there was no such loss. The inelastic branch starts at (Δ_{yl}, V_{max}) or (φ_{yl}, M_{max}), and ends at (Δ_u, V_u) or (φ_u, M_u). Both the lateral load V_u and the bending moment M_u are obtained by imposing an energetic equilibrium between the idealized bilinear diagram and the real envelope curve.

Table 4
Summary of test results.

Id	Specimen	μ	Bar buckling	Critical region l_{cr} (m)	l_{cr}/h
N1	NF00L05V2S100	2	Yes	0.35	1.35
N2	NF00L05V2S50	3	–	0.19	0.73
N3	NF00L05V1S50	3	Yes	0.16	0.62
N4	NF00L10V2S70	8	Yes	0.18	1.29
N5	NF00L05V3S50	2	–	0.30	1.04
N6	NF00L10V3S70	6	Yes	0.24	1.71
N7	NF30L05V2S100	2	Yes	0.20	0.77
N8	NF30L05V2S50	3	–	0.19	0.73
N9	NF60L05V2S100	3	Yes	0.24	0.92
N10	NF60L05V2S50	4	–	0.20	0.77
N11	NF60L05V2S600	2	Yes	0.35	1.35
N12	NF60L10V2S70	5	Yes	0.17	1.21
N13	NF60L10V1S70	6	–	0.17	1.21
N14	NF60L05V1S50	5	Yes	0.21	1.19

The ultimate ductility is defined in terms of displacements as $\mu_{\Delta u} = \Delta_u/\Delta_{yI}$; and in terms of curvatures as $\mu_{\varphi u} = \varphi_u/\varphi_{yI}$.

Table 5 shows the results of ductility in the specimens. Furthermore, the level of ductility reached based on the classification by the Spanish seismic code NCSR-02 [24] is included: high ductility ($\mu_{\Delta u} \geqslant 4$), medium ($4 > \mu_{\Delta u} \geqslant 3$), low ($3 > \mu_{\Delta u} \geqslant 2$), or no ductility ($2 > \mu_{\Delta u} \geqslant 1$). Fibrous specimens show low or medium levels of ductility. Specimens without steel fibres (Nonfibrous specimens) show medium to high levels except for NF60L05V2S600, which suffered a shear failure. Excepting specimens without fibres with $\lambda_V = 10.71$, the EC-8 [14] conservative expression that relates both types of ductility ($\mu_{\varphi u} = 2\ \mu_{\Delta u} - 1$) is fulfilled.

The column drift can be obtained as Δ_u/L_s ($L_s = 1500$ mm in this work). A direct relationship between column drift and ductility has been observed (Table 5). Thus, below 2% drift ductility is low, up to 3% is medium, and below 4% is high.

At each cycle i the energy dissipation can be defined as (Fig. 14):

$$E_i = \oint_A^B V\,d\Delta \tag{3}$$

The total energy dissipation during the test E_{hist} up to conventional failure is:

$$E_{hist} = \sum_{i=1}^{n} E_i \tag{4}$$

where n is the number of cycles applied to the specimen.

For the purpose of comparison, the normalized energy dissipation E_N was obtained as follows:

$$E_N = \frac{1}{V_{max} \cdot \Delta_{yI}} \sum_{i=1}^{n} E_i \tag{5}$$

Table 5 shows the results of E_N obtained for each specimen.

3.3. Strength capacity

Table 5 reports the maximum lateral load reached (V_{max}) and the maximum bending moment in the critical section (M_{max}) in each test. In both cases, the effects of own weight and second-order effects (for the calculation of the bending moment) have been considered.

A comparison between the experimental results and the method proposed by EC-2 [13] has been carried out. EC-2 [13] code recommends the use of the moment magnification method in order to take into account the second-order effects, which is based on the following factor δ_{ns}.

$$\delta_{ns} = 1 + \frac{\beta}{N_{cr}/N - 1} \tag{6}$$

where $\beta = \pi^2/12$ for a symmetric triangular distribution of the first order moment, N is the design value of the axial load, N_{cr} is the buckling load which is equal to $\pi^2 EI/l_p^2$, where EI is the nominal stiffness of the support and l_p is the effective buckling length. The nominal stiffness of the column EI is evaluated according to expression 5.21, section 5.8.7.3 EC-2 [13]. It is considered the semi-column as a cantilever support of 1.5 m length (Fig. 1) and an effective length $l_p = 3$ m. EC-2 [13] code does not take into account the effect of steel fibres to evaluate the nominal stiffness.

(a) NF0L5V2S100 (μ=2) (b) NF60L5V2S50 (μ=5) (c) NF60L5V2S600 (μ=2)

Fig. 12. Specimen behaviour at ultimate.

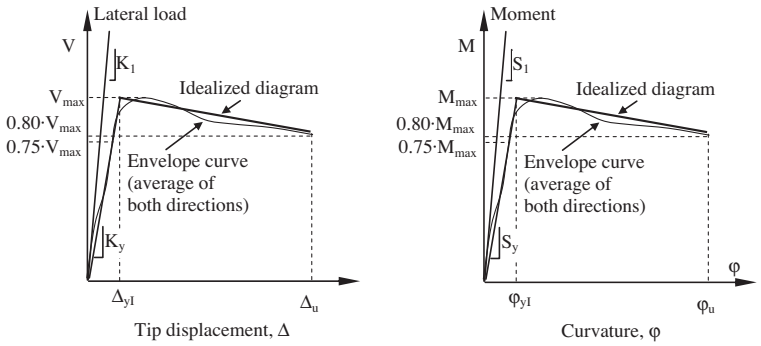

Fig. 13. Idealized curve definitions.

Table 5
Experimental results.

Id	Specimen	φ_{yI} (10^{-3} rad/m)	φ_u (10^{-3} rad/m)	$\mu_{\varphi u}$	Δ_{yI} (mm)	Δ_u (mm)	Drift Δ_u/L_s (%)	$\mu\Delta_u$	Displacement ductility (NCSR-02)	E_N	M_{max} (mkN)	$M_{max}/M_{EC\text{-}2}$	V_{max} (kN)	$V_{max}/V_{EC\text{-}2}$
N1	NF00L05V2S100	18.59	69.15	3.72	11.47	31.20	2.08	2.72	Low	7.19	71.68	1.01	85.81	1.11
N2	NF00L05V2S50	19.56	108.39	5.54	13.43	44.46	2.96	3.31	Medium	8.32	67.38	1.02	80.01	1.08
N3	NF00L05V1S50	22.31	150.39	6.74	14.57	52.73	3.52	3.62	Medium	15.28	47.14	0.96	63.50	1.02
N4	NF00L10V2S70	22.98	116.76	5.08	11.33	43.75	2.92	3.86	Medium	26.91	16.29	0.94	15.04	1.40
N5	NF00L05V3S50	14.31	48.24	3.37	8.73	18.08	1.21	2.07	Low	4.12	69.55	1.10	79.47	1.25
N6	NF00L10V3S70	15.51	41.25	2.66	14.00	33.18	2.21	2.37	Low	25.41	16.56	0.94	17.36	–
N7	NF30L05V2S100	13.49	63.95	4.74	10.92	34.93	2.33	3.20	Medium	9.81	71.25	0.99	80.97	1.02
N8	NF30L05V2S50	19.04	158.80	8.34	11.01	45.03	3.00	4.09	High	13.41	75.60	0.97	86.06	1.01
N9	NF60L05V2S100	20.80	112.34	5.40	11.45	38.57	2.57	3.37	Medium	8.58	70.83	0.96	83.79	1.01
N10	NF60L05V2S50	17.84	157.00	8.80	15.33	71.88	4.79	4.69	High	23.10	69.36	1.02	83.51	1.12
N11	NF60L05V2S600	22.98	75.59	3.29	14.48	31.42	2.09	2.17	Low	0.50	71.24	0.98	85.75	1.06
N12	NF60L10V2S70	26.26	324.32	12.35	10.72	52.63	3.51	4.91	High	48.15	17.35	0.95	13.47	1.39
N13	NF60L10V1S70	52.01	361.46	6.95	24.62	102.16	6.81	4.15	High	39.29	14.83	0.91	13.92	0.90
N14	NF60L05V1S50	27.28	159.34	5.84	19.08	73.25	4.88	3.84	Medium	28.25	53.16	0.89	69.92	0.93
Average error	–	–	–	–	–	–	–	–	–	–	–	0.97	–	1.10
Coefficient of variation (%)	–	–	–	–	–	–	–	–	–	–	–	5.4	–	14.3

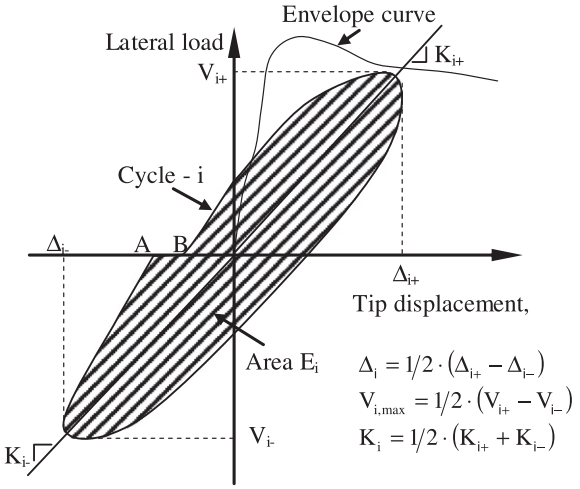

Fig. 14. Energy dissipation.

In order to evaluate the ultimate bending moment, the parabola-rectangle diagram for concrete in compression has been used (Section 3.1.7 EC-2 [13]). The safety factor γ_c and the sustained loads coefficient α_{cc} are assumed to be "1" for experimental tests. EC-2 [13] code does not take into account the effect of the residual flexural tensile strength of the steel fibres in the evaluation of the ultimate bending moment. As the formulation to evaluate the ultimate bending moment in a section without steel fibres is the same in EC-2 [10] code and in MC [34], the effect of the residual flexural tensile strength is considered by a rectangular diagram (rigid-plastic model) according to MC [21] (Section 5.6.4). The ultimate residual strength is determined as $f_{R3}/3$ for all tests (Table 3). The safety factors are taken equal to one.

Table 5 shows the results obtained for all the specimens both for the maximum bending moment M_{max} and the maximum lateral load V_{max}. It has not been possible to obtain the maximum lateral load V_{max} for specimen NF00L05V3S50 because the axial load achieved was greater than the buckling load N_{cr} obtained with the simplified method.

The prediction of the maximum bending moment (M_{max}) according to EC-2 [10] code is quite accurate and slightly unsafe. EC-2 [10] code is much more safe when it is obtained the maximum lateral load (V_{max}). Regarding the maximum bending moment, the average ratio is 0.97 and the coefficient of variation is 5.4%, and regarding the maximum load, the average ratio is 1.10 and the coefficient of variation is 14.3%. There is a greater loss of accuracy for sections or columns with steel fibres.

4. Analysis of results

4.1. Effects of confinement and inclusion of steel fibres

Fig. 15 shows the results for the analysis of the effects of confinement and the inclusion of fibres. The ductility ($\mu_{\Delta u}$, $\mu_{\varphi u}$), and the strength capacity (V_{max}, M_{max}) are evaluated as a function of the residual flexural tensile strength f_{R3} (see Table 3)

There are seven specimens for comparison: NF60L05V2S600, NF00L05V2S100, NF30L05V2S100, NF60L05V2S100, NF00L05V2S50, NF30L05V2S50, and NF60L05V2S50. The numerical results are shown in Table 5. For all the selected specimens, slenderness is 5.77, average concrete compressive strength 32.84 MPa, and average relative normal force 0.36. The values are presented in all cases as a function of the transverse reinforcement spacing: 600, 100 and 50 mm. This corresponds to confinement effectiveness factors of 0.01, 0.04 and 0.12 respectively. Moreover, Fig. 15b shows the predicted ductility according to EC-8 [14]:

$$\mu_{\varphi u} = \frac{\alpha \cdot \omega_\omega + 0,035}{30 \cdot \nu_d \cdot \varepsilon_{sy,d}} \cdot \frac{b_o}{b_c} \tag{7}$$

where ν_d is the reduced axial compressive force, $\varepsilon_{sy,d}$ is the deformation in the steel for the design stress f_y, b_c is the width of the cross-section, and b_o is the width of the confined core (to the centreline of the hoops). Safety factors are taken to equal one.

The displacement ductility increases with the confinement effectiveness factor, as expected (Fig. 15a). Thus, in fibrous specimens, with double transverse reinforcement ratio, there was a 30% increase in the displacement ductility (NF00L05V2S100 vs. NF00L05V2S50). The series corresponding to $\alpha \cdot \omega_\omega = 0.04$ ($s_t = 100$ mm) shows that steel fibres improve the deformation capacity of the specimen. Therefore, a fibre content increase of 30 kg/m^3 produces a 25% increase in ductility (NF00L05V2S100 vs. NF30L05V2S100). However, an increase of the fibre content from 30 to 60 kg/m^3 represents a slight 5% improvement over the previous case (NF30L05V2S100 vs. NF60L05V2S100). Steel fibres improve the concrete postpeak behaviour, and delay the effect of

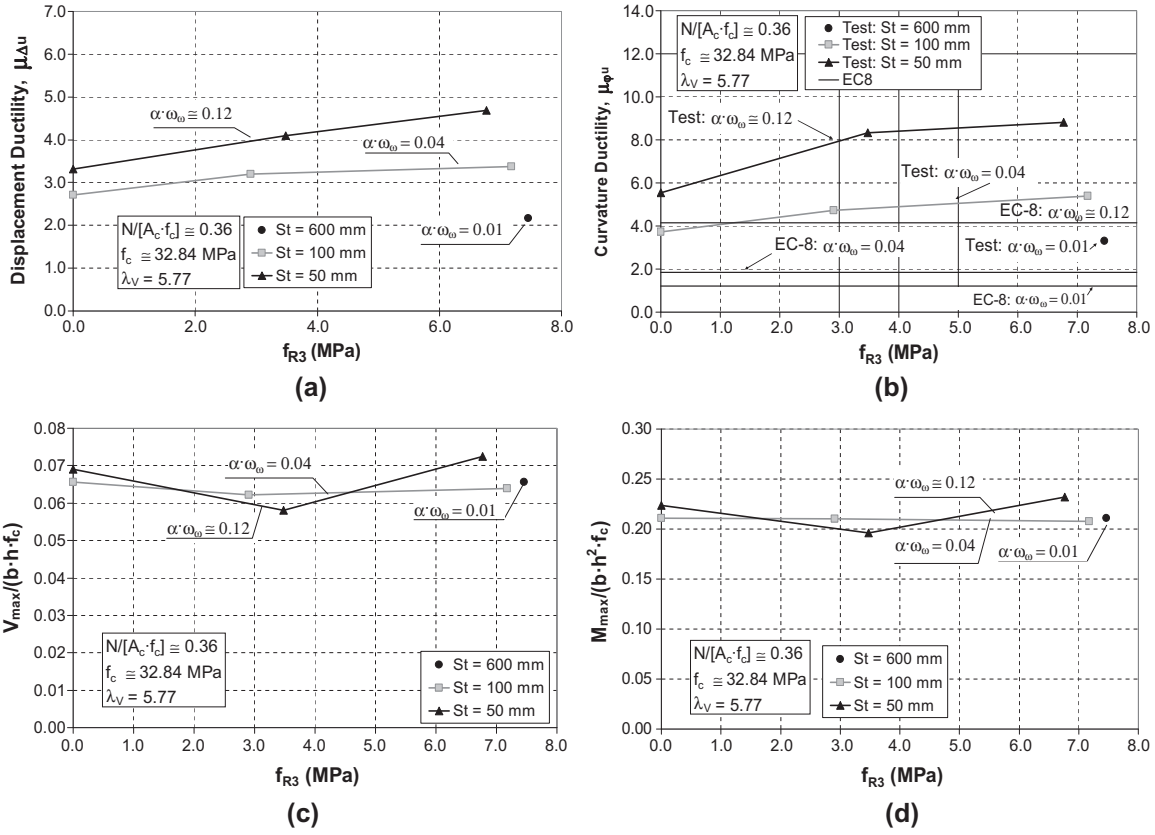

Fig. 15. Deformation and strength capacity: effect of transverse reinforcement and steel fibres.

concrete spalling. Hence, the section curvature at the plastic hinge increases without a significant loss of strength capacity. However, a 60 kg/m^3 fibre content does not increase ductility significantly in comparison to 30 kg/m^3, because the bars in compression buckle and limit the deformation capacity of the specimen. Even though fibres delay concrete spalling, buckling cannot be avoided.

For $\alpha \cdot \omega_\omega = 0.12$ ($s_t = 50$ mm) series, 30 kg/m^3 of fibres show an improvement in ductility of 23% (NF00L05V2S50 vs. NF30L05 V2S50), while 60 kg/m^3 represents an improvement over 30 kg/m^3 of 16% (NF30L05V2S50 vs. NF60L05V2S50). No buckling in the reinforcement is observed, and ductility $\mu_{\Delta u}$ improves with the residual tensile strength f_{R3} proportionally. Moreover, specimen NF60L05V2S600 ($s_t = 600$ mm and 60 kg/m^3 of fibres) shows the lowest ductility $\mu_{\Delta u}$ of all the specimens analyzed in this section. In this case, the possible beneficial effect of the fibres does not occur because of the compression reinforcement buckling, thus resulting in a significant loss of strength capacity in the postpeak behaviour.

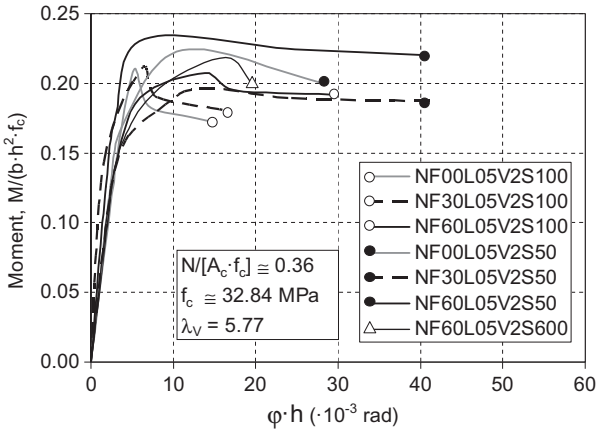

Fig. 16. Bending moment–curvature envelope: effect of transverse reinforcement and steel fibres.

The curvature ductility ($\mu_{\varphi u}$) shows the same tendency as the displacement ductility $\mu_{\Delta u}$ (Fig. 15a and b), and is on the safe side compared with the expected value of ductility according to EC-8 [14] (this code does not take into account the favourable effect of the inclusion of steel fibres into the concrete mixture). Since the ideal elastic curve of all specimens is almost the same (on average $\varphi_{yI} = 18.89 \times 10^{-3}$ rad/m, CV = 15%)), the increase in $\mu_{\varphi u}$ is due to the increase in the ultimate curvature (φ_u), which occurs thanks to the improvement in the concrete postpeak behaviour. The latter occurs when the confinement is increased or when steel fibres are included, while the reinforcement does not buckle, and therefore, major distortions in the reinforcement and in the concrete are achieved in this cross-section.

The mean value of the nondimensional lateral load $V_{max}/(b \cdot h \cdot f_c)$ is 0.07 with a CV = 7.16% for the seven specimens analyzed (Fig. 15c). The scatter of the results is reasonable in this type of laboratory test. Consequently, no significant variation in the lateral load due to the confinement or the inclusion of steel fibres is found.

Finally, the mean value of the nondimensional ultimate moment, $M_{max}/(b \cdot h^2 \cdot f_c)$ is 0.21 with a CV = 5.37% for all of the seven specimens analyzed (Fig. 15d). Once again the scatter of results is reasonable for this type of test. Results show the same tendency as for the case of maximum load. Moreover, the ultimate bending moment does not increase due to the effect of confinement or the inclusion of fibres. It has been observed that after spalling of

concrete cover, the capacity of the confined core is less than the capacity of the full unconfined section. Furthermore, the longitudinal reinforcement is in tension when the bending moment is maximum, and there is no evidence of a significant improvement in the sectional strength capacity thanks to the residual tensile strength provided by the steel fibres.

Fig. 16 shows the bending moment-curvature diagrams for the nondimensional envelope curves. Specimens NF30L05V2S100 and NF00L05V2S100 (both with s_t = 100 mm) suffered concrete spalling, and therefore, a loss of strength capacity. However, in specimen NF60L05V2S100 the loss is less important. Specimens with s_t = 50 mm do not show any loss. Finally, in the specimen with s_t = 600 mm (NF60L05V2S600), concrete spalling implied the end of the test.

According to Table 5, the tendency in comparison to the normalized energy dissipation (E_N) is the same as that obtained for $\mu_{\Delta u}$. The specimen with the worst behaviour is NF60L05V2S600. Specimens NF00L05V2S100, NF30L05V2S100, and NF60L05V2S100, with $\alpha \cdot \omega_\omega$ of 0.04 (s_t = 100 mm) volumetric mechanical ratio of confinement, show similar values in spite of the increase of fibre content. However, for specimens NF00L05V2S50, NF30L05V2S50, and NF60L05V2S50, with $\alpha \cdot \omega_\omega$ of 0.12 (s_t = 50 mm), E_N increases with the amount of steel fibres, so that specimen NF60L05V2S50 shows the best energy absorption capacity.

4.2. Effect of the axial load and the column slenderness

Fig. 17 shows the results for the analysis of the effect of the axial load and the column slenderness in comparison with the deformation capacity ($\mu_{\Delta u}$, $\mu_{\varphi u}$), and the strength capacity (V_{max}, M_{max}) as a function of the relative normal force $N/(b \cdot h \cdot f_c)$. The results corresponding to specimens with no fibres and with 60 kg/m^3 of fibre content are presented. The following specimens are analyzed: five without fibres (NF00L05V1S50, NF00L05V2S50, NF00L05V3S50, NF00L10V2S70, and NF00L10V3S70), and four with fibres (NF60L05V1S50, NF60L05V2S50, NF60L10V1S70, and NF60L10V2S70). The numerical results are shown in Table 5. Results are presented by type of concrete (with or without fibres) and by column slenderness in all cases. Furthermore, the value of ductility according to Eq. (5) is shown in Fig. 17b.

There are no ductility predictions for the most slender specimen (λ_V = 10.71) without axial fibres and a relative normal force of 0.10. However, similar values to those recorded for the specimens with the same axial load level (NF00L05V1S50 and NF60L05V1S50) are expected, given the fact that second-order effects are not important.

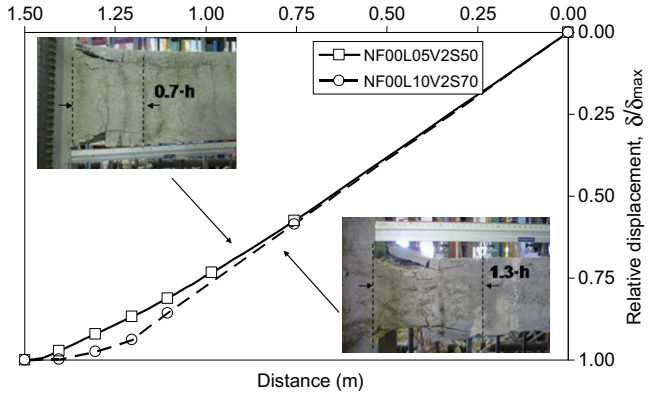

Fig. 18. Relative displacement of the column. Slenderness effect.

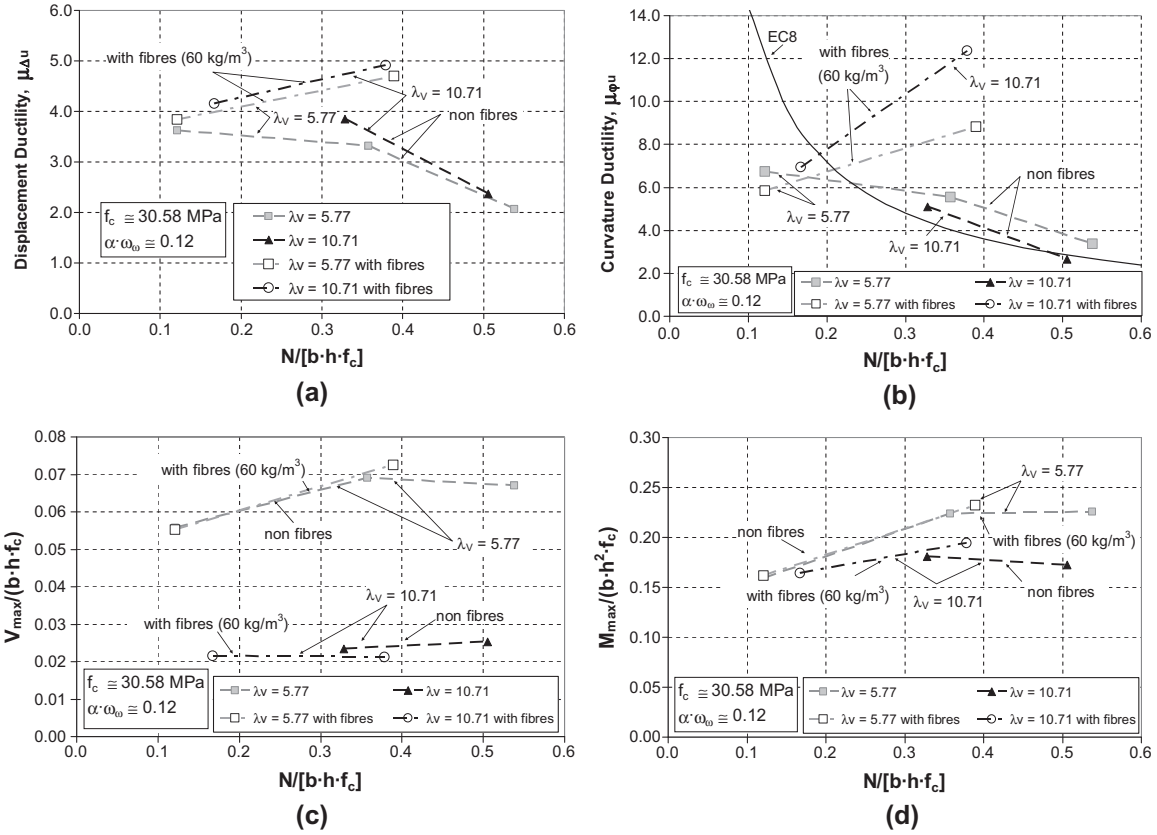

Fig. 17. Deformation and strength capacity: effect of slenderness, axial load level and steel fibres.

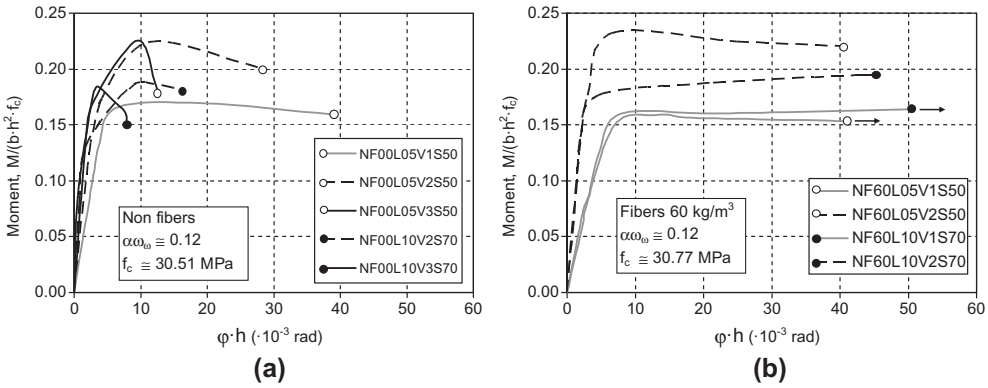

Fig. 19. Bending moment-curvature envelope: effect of slenderness and axial load level: (a) non-fibres and (b) fibres.

The effect of axial load in comparison to the displacement ductility $\mu_{\Delta u}$ is analyzed (Table 5 and Fig. 17a). In all cases ductility increases with the axial load level in columns with steel fibres (NF60L05V1S50 and NF60L05V2S50; NF60L10V1S70 and NF60L10V2S70). In contrast, nonfibrous specimens show that $\mu_{\Delta u}$ varies depending on the slenderness and the relative normal force. Thus, for the case with minimum slenderness ($\lambda_V = 5.77$) ductility decreases while the axial load level increases (NF00L05V1S50, NF00L05V2S50 and NF00L05V3S50). For the case with maximum slenderness ($\lambda_V = 10.71$), and assuming that the value of $\mu_{\Delta u}$ for a relative normal force is similar to that of the specimen NF00L05V1S50 mentioned earlier, ductility keeps practically constant up to an axial load level (around 0.35), and ductility decreases beyond this level (NF00L10V2S70 and NF00L10V370). It is worth noting that previous researchers [23,36,5] have also found that ductility decreases with the axial load level in nonfibrous columns with low slenderness ($\lambda_V < 6$). This is also observed when analyzing curvature ductility (Table 5 and Fig. 17b).

The curvature ductility increases with the longitudinal reinforcement ratio in the case of sections with symmetrical reinforcement, as shown theoretically by Bai and Au [6] and experimentally observed in Table 5 and Fig. 17b. Thus, in nonfibrous specimens, the cross-section with $\rho_l = 1.74\%$ in the lowest slenderness column ($\lambda_V = 5.77$) shows the highest curvature ductility. However, when studying the displacement ductility experimentally the opposite behaviour occurs for a medium axial load level of 0.35. (NF00L05V2S50 vs. NF0L10V2S7, Fig. 17a). For low (of 0.10) or high (of 0.55) levels this effect does not occur. This behaviour depends on the importance of the second-order effects and the ductility of the section: if the axial force is low (0.1), the second-order effects are unimportant and the behaviour in displacements to be expected is similar to that observed at section level; if the axial force is medium (0.35), the second-order effects are important, and the section is also sufficiently ductile; finally, if the axial load level is high (0.55), the section is not ductile enough, and despite second-order effects being important.

Therefore, slenderness will have an influence on column ductility if the second-order effects are important, the section has a ductile enough behaviour at ultimate, and failure occurs due to the capacity of the materials, not because of column instability. Thus, even though the most slender specimen (NF00L10V2S70) may have lower curvature ductility than another specimen (NF00L05V2S50), second-order loads are so important that the total bending moment diagram changes, increasing the potential yielded area. Fig. 18 shows the deformed shape of the instrumented side corresponding to specimens NF00L05V2S50 and NF00L10V2S70 at conventional failure. The vertical axis represents relative displacements between the lateral displacement of the section (δ) and the maximum displacement recorded in the clamped section (δ_{max}). In the most slender specimen (NF00L10V2S70), a significant curvature concentration in the critical length of the column can be observed (Fig. 18).

Fig. 19 shows the bending moment-curvature diagrams for the nondimensional envelope curves. Moreover, the typical behaviour of two sections with different longitudinal reinforcement ratios (without fibres), and subjected to a variation of axial force, can be observed (Fig. 19a). Conventional failure is reached only for high axial load levels due to limitations of the structural experimental test. Fig. 19b shows the diagrams corresponding to test specimens with steel fibres, in which a postpeak descending branch has not been observed.

Ductility curvature ($\mu_{\varphi u}$) decreases with axial force and longitudinal reinforcement ratio in nonfibrous specimens (Fig. 17b). Nevertheless, this tendency is the opposite in specimens with steel fibres (NF60L05V2S50, NF60L10V1S70, NF60L05V1S50 and NF60L10V2S70), showing the same tendency in comparison with the displacement ductility. The bending moment–curvature diagram (Fig. 19b) shows a nearly elastic, perfectly-plastic behaviour for these specimens. Therefore, the decrease in the postpeak behaviour of the load-displacement diagram (V–Δ) is due to the P–Δ effects, rather than a loss of strength capacity due to material degradation (Figs. 10f and 11e–g).

EC-8 [14] code is on the safe side for medium to high axial load levels in specimens without steel fibres (Fig. 17b). When axial force is low the conventional failure has not been achieved in the experimental tests, despite the fact that a theoretical ductility value can be obtained according to the codes. Conventional failure has not been reached for fibrous specimens either, and codes are very conservative if the axial load level is medium.

Regarding the maximum load and bending moment (Fig. 17c and d), a similar strength capacity in specimens with and without fibres is shown, while the other parameters are kept constant. The other tendencies are as expected when the longitudinal reinforcement ratio, the slenderness, and the axial load level are varied.

Finally, the tendency observed in comparison with the normalized energy dissipation (E_N) is the same as that shown for the displacement ductility ($\mu_{\Delta u}$).

5. Conclusions

In this study the following conclusions have been drawn:

- The inclusion of steel fibres into the concrete mixture delays concrete cover spalling and buckling of the longitudinal reinforcement bars in compression, reduces the critical region length, which involves minor damage in the area where the plastic hinge is likely to occur, and improves curvature ductility increasing the energy dissipation.

- There has not been an increase in the maximum strength capacity with the inclusion of steel fibres. This suggests that the favourable effect of the residual flexural tensile strength f_{R3} decreases with the cyclic load applied.
- A descending branch in the bending moment-curvature diagrams of the specimens with steel fibres was not detected, indicating that the decrease in the load-displacement diagrams (V–Δ) is due to P–Δ effects.
- To ensure the required deformation capacity it is necessary to prevent the longitudinal reinforcement buckling along the length where a plastic hinge may be developed. To this end, there must be fixed appropriate transverse reinforcement spacing depending on the type of concrete (with or without fibres), the required deformation capacity, and the diameter of the longitudinal reinforcement.
- The transverse reinforcement was anchored with 135° hooks into the concrete core according to ACI-318 (08) [1], and was effective (the opening of stirrup hooks has not been observed). Therefore, there was no decrease in deformation capacity as a result of a loss of confinement.
- Ductility will only depend on the slenderness if the second-order effects are important, the behaviour of the section is sufficiently ductile, and the material specimens reach their maximum strength, but not the instability of the column.
- In the case of nonfibrous concrete, the displacement and curvature ductility decrease with the axial load applied in low slender columns, while in high slender supports ductility is almost constant up to a certain level of relative normal force, and beyond this decreases.
- The deformation capacity obtained in columns with no fibres is similar both for low and high axial load levels, while it increases for the highest slender columns for medium load level.
- The ratio between the critical region length and the total depth of the section l_{cr}/h increases with the column slenderness, the axial load level, and the transverse reinforcement spacing.
- EC-8 [14] ductility predictions are on the safe side for medium to high axial load levels, while they are on the unsafe side for low axial load levels.
- Ductility predictions according to EC-8 [14] are conservative for fibrous specimens.

Acknowledgments

The authors of this work wish to thank the research bureau of the Spanish Ministry of Science and Innovation and the Plan E, for the funding of the Project BIA 2008-03734 and BIA 2009-10207.

References

[1] ACI 318-08. Building code requirements for reinforced concrete. American Concrete Institute, Detroit; 2008.
[2] ACI 544.4R-88. Design considerations for steel fiber reinforced concrete (reapproved 2009). American Concrete Institute, Detroit; 2009.
[3] ACI-ASCE Committee 441. High strength concrete columns: state of the art. Am Concr Inst Struct J 1997;94(3):325–35.
[4] Aoude H, Cook WD, Mitchell D. Axial load response of columns constructed with fibres and self-consolidating concrete. ACI Struct J 2009;106(03):349–57.
[5] Bae S, Bayrak O. Seismic performance of reinforced concrete columns: P–Δ effect. ACI Special Publ 2006;236:61–80.
[6] Bai ZA, Au FTK. Ductility of symmetrically reinforced concrete columns. Mag Concr Res 2009;61(5):345–57.
[7] Barrera AC, Bonet JL, Romero ML, Miguel PF. Experimental tests of slender reinforced concrete columns under combined axial load and lateral force. Eng Struct 2011;33(12):3676–89.
[8] Berry M, Parrish M, Eberhard M. PEER structural performance database user's manual (www.ce.washington.edu/~peera1). Pacific Earthquake Engineering Research Center, University of California, Berkeley; 2004.
[9] Campione G, Fossetti M, Papia M. Behavior of fibre-reinforced concrete columns under axially and eccentrically compressive loads. ACI Struct J 2010;107(03):272–81.
[10] CEB-FIP Task Group 7.2. Bulletin 25, State of art report (Displacement-based seismic design of reinforced concrete buildings). Lausanne-Switzerland; 2003.
[11] Comisión Permanente del Hormigón, Ministerio de Fomento, Code on Structural Concrete EHE-08. Spanish Goverment, Madrid; 2008.
[12] Consiglio Nazionale delle Ricerche "Istruzioni per la Progettazione, l'esecuzione ed il controllo di strutture di Calcestruzzo Fibroinforzato" CNR-DT 204/2006.
[13] European Committee for Standardization. Eurocode 2: design of concrete structures – Part 1: general rules and rules for buildings (EN 1992-1-1); 2004.
[14] European Committee for Standardization. Eurocode 8: design of structures for earthquake resistance – Part 1: general rules, seismic actions and rules for buildings (EN 1998–1); 2004.
[15] Ezeldin AS, Balaguru PN. Normal and high strength fibre reinforced concrete under compression. ASCE J Mater Civil Eng 1992;4(4):415–29.
[16] Fanela DA, Naaman AE. Stress–strain properties of fibre reinforced mortar in compression. ACI J 1985;82(4):475–83.
[17] Federal Emergency Management Agency, FEMA-P-750. NEHRP recommended provisions for new buildings and other structures. Washington, DC; 2009.
[18] Foster SJ. On behaviour of high-strength concrete columns: cover spalling, steel fibres and ductility. ACI Struct J 2001;98(04):583–9.
[19] Ho JCM, Pam HJ. Inelastic design of low-axially loaded high-strength reinforced concrete columns. Eng Struct 2003;25:1083–96.
[20] Hwang SK, Yun HD. Effects of transverse reinforcement on flexural behaviour of high-strength concrete columns. Eng Struct 2004;26(1):1–12.
[21] International Federation for Structural Concrete (fib) "Model Code 2010. First Complete Draft" Bulletin 55 and 56; March 2010.
[22] Khoury SS, Sheikh SA. Behavior of normal and high strength confined concrete columns with and without stubs. Research Report No. UHCEE 91-4, University of Houston, Houston, Tex.; 1991.
[23] Légeron F, Paultre P. Behavior of high-strength concrete columns under cyclic flexure and constant axial load. ACI Struct J 2000;97(4):591–601.
[24] Ministerio de Fomento. Norma de construcción sismorresistente: parte general y edificación (NCSR-02). Spanish Goverment, Madrid; 2002.
[25] Nataraja MC, Dhang N, Gupta AP. Stress–strain curves for steel fibre reinforced concrete under compression. J Cem Compos 1999;21:383–90.
[26] Pam HJ, Ho JCM. Length of critical region for confinement steel in limited ductility high-strength reinforced concrete columns. Eng Struct 2009;31:2896–908.
[27] Panagiotakos TB, Fardis MN. Deformations of reinforced concrete members at yielding and ultimate. ACI Struct J 2001;98(2):135–48.
[28] Paultre P, Eid R, Langlois Y, Lévesque Y. Behaviour of steel fibre-reinforced high-strength concrete columns under uniaxial compression. ASCE J Struct Eng 2010;136(10):1225–35.
[29] Paultre P, Légeron F, Mongeau D. Influence of concrete strength and transverse reinforcement yield strength on behavior of high-strength concrete columns. ACI Struct J 2001;98(4):490–501.
[30] Priestley MJN, Park R. Strength and ductility of concrete bridge columns under seismic loading. ACI Struct J 1987;84(61):76.
[31] Standards New Zealand. Concrete structures standard part 2 – commentary on the design of concrete structures NZS 3101: Part 2:2006; 2006.
[32] UNE-EN 10002-1. Metallic materials: tensile testing. Part 1: method of test at ambient temperature. AENOR, Asociación Española de Normalización y Certificación; 2002.
[33] UNE-EN 12390-3. Ensayos de hormigón endurecido–Parte 3: determinación de la resistencia a compresión de probetas. Asociación Española de Normalización y Certificación; 2000.
[34] UNE-EN 14651:2007. Método de ensayo para hormigón con fibras metálicas. Determinación de la resistencia a la tracción por flexión (límite de proporcionalidad (LOP), resistencia residual". Asociación Española de Normalización y Certificación; 2007.
[35] UNE-EN 197-1:2000. Cemento – Parte 1: Composición, especificación y criterio de conformidad para cementos comunes. Asociación Española de Normalización y Certificación; 2000.
[36] Wang Q, Zhao G, Lin L. Effect of axial load ratio and stirrups volume ratio on ductility of high-strength concrete columns. ACI Special Publ 1994;149(24):433–48.
[37] Yamashiro R, Siess CP. Moment-rotation characteristics of reinforced concrete members subjected to bending, shear, and axial load. Civil engineering studies, structural research series no. 260, University of Illinois, Urbana; 1962.